JOURNAL OF MATERIALS SCIENCE 30 (1995) 4912–4925

Remelting phenomena in the process of splat solidification

B. KANG, J. WALDVOGEL, D. POULIKAKOS
Mechanical Engineering Department, University of Illinois at Chicago, Chicago, IL 60607, USA

A combined theoretical and experimental study is reported which investigates remelting phenomena during the splat cooling of two liquid-metal droplets impacting sequentially on a substrate. Under conditions of sufficiently high superheat it was proposed theoretically and demonstrated experimentally that an initial deposit is remelted by the subsequent impact of molten material. It is shown that the amount of superheat as well as the variation of thermophysical properties, particularly the latent heat and the melting temperature, influence the degree of remelting. Experimental findings supported to a certain extent the theoretical model assumptions that the splats could be represented by thin discs and that the heat transfer and solidification within the splat propagates in the axial direction only. However, the experiments showed that these assumptions are better suited for the central region of the splat. The occurrence of remelting often depended on the radial location for a given amount of superheat. For most part, the splat exhibited globular microstructure. Lamellar structures were observed near the top and the periphery of the splat, indicating slower cooling rates at these locations. The theoretical model constituted a good compromise between accuracy and simplicity and predicted the correct trends of the remelting phenomenon.

Nomenclature

c	Specific heat ($J\,kg^{-1}\,K^{-1}$)
d	Diameter of a spherical droplet (mm)
D	Diameter of the splat (mm)
h_a	Convective heat-transfer coefficient ($W\,m^{-2}\,K^{-1}$)
h_c	Contact heat-transfer coefficient ($W\,m^{-2}\,K^{-1}$)
H	Height of the splat (mm)
I	Number of nodes in the axial direction in a splat
k	Thermal conductivity ($W\,m^{-1}\,K^{-1}$)
K_f	Freezing kinetics coefficient ($m\,s^{-1}\,K^{-1}$)
L	Latent heat ($J\,kg^{-1}$)
M	Number of nodes in the radial direction in a substrate
N	Number of nodes in the axial direction in a substrate
r	Radial coordinate (mm)
R	Radius of a splat (mm)
Δr	Increment of radial coordinate (mm)
t	Time (s)
t'	Time lapsed since the solidification of the bottom splat starts
T	Temperature (°C)
T_f	Equilibrium freezing temperature (°C)
T_0	Initial temperature of the top splat (°C)
T_∞	Initial temperature of the substrate or ambient air temperature (°C)
V	Interface velocity ($m\,s^{-1}$)
z	Axial coordinate (mm)
Δz	Increment of axial coordinate (mm)
ξ	Spread factor
ρ	Density ($kg\,m^{-3}$)

Superscripts

l	Liquid
m	Index taking on the values s for solid or l for liquid
s	Solid

Subscripts

b	Bottom of control volume containing the freezing interface
i	Interface
j	Index taking on the values 1 for the first (bottom) splat or 2 for the second (top) splat
sup	Amount of superheat of the second splat
t	Top of control volume containing the freezing interface
1	First splat
2	Second splat

1. Introduction

Splat-quenched solidification involves the impingement, spreading, and ensuing solidification of liquid-metal droplets on a solid substrate. In the case of splat quenching of an alloy from the liquid state, the

0022–2461

potential exists for novel non-equilibrium phases to be captured. Because the atomic mobility in a liquid is far greater than in a solid, the quenching rate must be very fast to arrest a non-equilibrium state residing in the liquid phase. The cooling rates imposed on the melt in the process of splat quenching are typically many orders of magnitude faster than conventional solidification methods. In the early stages of spray deposition processes, splat-quenched solidification occurs. To this end, consecutive generations of entirely liquid molten droplets impact upon a completely solidified surface [1–5] because heat transfer (principally conduction) away from the deposition layer is capable of removing heat much faster than it is deposited by the molten material.

Jones [1] and Anatharaman and Suryanarayana [6] have summarized the early progress of the splat-quenching technique. Predecki *et al.* [7] were able to estimate cooling rates, the splat–substrate heat-transfer coefficient and solidification rates, by assuming that the cooling of the splat was Newtonian (no temperature gradients were established within the splat).

Brower *et al.* [8] performed a comparative study of the relative cooling rate and its effect on microstructure for cooling imposed by gas quenching, liquid quenching, chill casting, and splat quenching. They found that typical cooling rates were $1–10\,^{\circ}C\,s^{-1}$ for gas quenching, $30–200\,^{\circ}C\,s^{-1}$ for liquid quenching, $10^{3}–10^{4}\,^{\circ}C\,s^{-1}$ for chill casting, and $10^{5}–10^{6}\,^{\circ}C\,s^{-1}$ for splat quenching. They also investigated the effect of splat thickness on the cooling rate and determined that the cooling rate of the splat would be increased by faster thinning of the melt.

Scott [9] measured the average and maximum cooling rate exhibited by aluminium copper alloy splats quenched on copper and glass (soda glass) substrates. He found the surprising result that the cooling rate of a splat on the glass substrate was higher than the cooling rate of the same splat on a copper substrate. He suggested that the thermal contact between the splat and the substrate was much better for the glass substrate because he noticed that the splats had melted the surface of the glass substrate slightly, thereby improving the thermal contact.

Wang and Matthys [10, 11] calculated theoretically the interface velocity with and without undercooling of the melt using a one-dimensional conduction model which treated the splat as a thin disc in contact with a semi-infinite substrate. With undercooling, the velocity of the interface decreased rapidly as the freezing front advanced. Without undercooling, the velocity of the interface was heat-transfer limited, yielding a more moderate change in interface velocity. The quality of thermal contact between splat and substrate was influential in sustaining the interface velocity in an undercooled melt.

Relevant to the splat-quenching process was the work of Shingu and Ozaki [12] who numerically investigated rapid solidification occurring by conduction cooling. Roshar and Epstein [13] studied theoretically the simultaneous kinetic and heat-transfer limitations in the crystallization of highly undercooled melts. Evans and Greer [14] developed a one-dimensional numerical solution for the rapid solidification of an alloy melt in order to investigate solute trapping. They found that the heat extraction rate seriously affected the freezing interface velocity and the degree of solute trapping. Changes in initial alloy composition slightly altered the interface temperature; however, this change in temperature did not have a large effect on the diffusivity of the liquid so as to alter substantially the amount of solute trapping.

Bennet and Poulikakos [15] presented a theoretical and experimental study on splat cooling focusing on the heat-transfer aspects of this process and on the identification of parameters affecting the heat-transfer mechanism. They found that a two-dimensional conduction model for the substrate coupled with a one-dimensional conduction model in the splat, accounting for the freezing process in the splat and the solidification kinetics agreed well with the trends observed in the experimental part of their study. Kang *et al.* [16] studied the problem of solidification of two liquid-metal droplets impacting sequentially on a solid surface. They reported that the solidification of the second droplet exhibited markedly lower cooling rates compared to the first droplet. As a result, the grain structure of the top of a two-droplet splat was significantly coarser than that of the bottom. They also demonstrated that the two-dimensional nature of the conduction phenomenon in the substrate should not be neglected.

The work presented in this paper aimed to improve and extend our understanding of the rapid solidification of a splat formed by two liquid-metal droplets quenched sequentially one on top of the other on a substrate. Because we were interested in the splat-cooling regime, the impact of the second droplet took place after the first droplet had solidified completely. The main goal of this study was to examine and quantify the *remelting* of the first droplet and the subsequent solidification of the molten material. In doing so, conclusions have been drawn concerning the effect of material properties and the amount of initial superheat on the depth of the remelted zone and the subsequent microstructural and macrostructural impact. This study is divided into two parts. First, a theoretical heat-transfer model of the remelting and solidification processes is outlined and the results of numerical simulations are provided. Next, an experiment is reported in which two liquid-metal droplets are deposited in succession on a substrate. Micrographs are presented which illustrate the remelting of the initial deposit and its effect on microstructure.

2. Mathematical model

The theoretical part of the study consists of an approximate heat-transfer model of the remelting of a pre-existing splat by the impaction of another hot droplet and the successive solidification of the molten region. Invoking a simple order of magnitude analysis it can be shown that the time scale of the spreading process of a droplet impacting on a surface is shorter than the time scale of the heat-transfer process from the splat to the substrate. This result

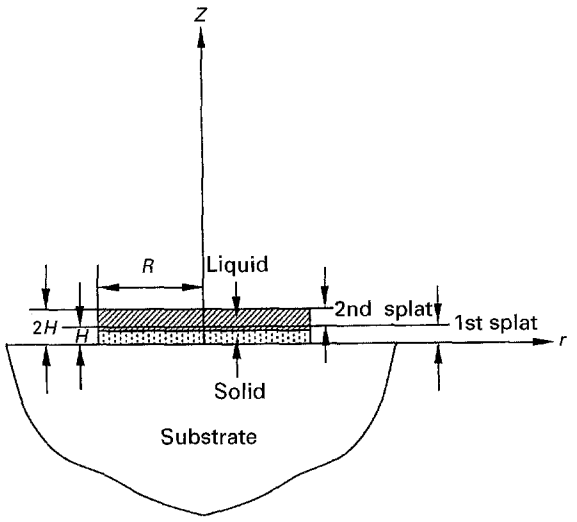

Figure 1 Schematic diagram of the system of interest.

practically implies that the droplets forming the splat spread first and cool down subsequently. To construct a relatively simple and easy to use model of the solidification process, we make use of the aforementioned result and model each droplet in the splat as a thin metal disc initially in the solid phase for the first splat, and in the liquid phase for the second splat. The simplification of modelling a splat as a thin metal disc has been used successfully in earlier investigations of single-droplet splats [10, 11, 15–18]

Fig. 1 shows a schematic drawing of the model of a two-droplet splat according to the aforementioned simplifications. The exact dimensions of each disc are determined from the experiments, as will be discussed in detail in Section 4. The bottom splat has already completed its solidification process and in a short time the second droplet with a certain amount of superheat is suddenly brought into contact with the bottom splat. With a high value of superheat, the temperature of the top surface of the bottom splat exceeds the melting temperature of the splat at the moment of the contact. Remelting of the bottom splat ensues from the top surface and progresses downwards until the velocity of the interface reaches zero. After a short time for the undercooling of the interface, the solidification of the remelted region ensues and progresses upwards until the freezing interface reaches the top of the bottom splat. In the case of low superheat, the temperature of the top surface of the bottom splat increases from the moment of contact but never exceeds the melting temperature of the splat, and no remelting occurs.

Owing to the fact that the thickness to diameter ratio of the splat is very small (typically of the order of 0.01), the heat-conduction process in the splat is practically unidirectional. Earlier studies of the heat-conduction process in a single-droplet splat [10, 11, 15, 16] have shown that neglecting the effect of radial conduction in the splat has minimal impact on the resulting temperature field. On the other hand, the present model will account for both radial and axial conduction in the substrate according to the recommendations given elsewhere [15, 16].

Following the above discussion, the heat conduction equation in both the first droplet and the second droplet in the splat reads

$$(\rho c)_j^m \frac{\partial T_j^m}{\partial t} = \frac{\partial}{\partial z}\left(k_j^m \frac{\partial T_j^m}{\partial z}\right) \tag{1}$$

where the subscript j takes on the values 1 or 2 corresponding to the first (bottom) or the second (top) disc and the superscript m takes on the values s or l denoting solid or liquid region. The temperature is denoted by T, the time by t, the axial coordinate by z (Fig. 1), and the density, specific heat, and the thermal conductivity of the splat material by ρ, c and k, respectively. The heat conduction equation in the substrate is

$$\rho c \frac{\partial T}{\partial t} = k\left(\frac{\partial^2 T}{\partial r^2} + \frac{1}{r}\frac{\partial T}{\partial r} + \frac{\partial^2 T}{\partial z^2}\right) \tag{2}$$

where the notation is analogous to what was defined above with the added clarification that r stands for the radial coordinate (Fig. 1).

The initial conditions for the splat and the substrate are

$$T_1^s(z, t = 0) = T_f - \Delta T_1 \tag{3}$$

$$T_2^l(z, t = 0) = T_0 = T_f + \Delta T_{sup} \tag{4}$$

$$T(r, z, t = 0) = T_\infty \tag{5}$$

The boundary and matching conditions accompanying the above are

$$T(r \to \infty, z = 0, t) = T_\infty \tag{6}$$

$$T(r, z \to -\infty, t) = T_\infty \tag{7}$$

$$\left(-k_2^l \frac{\partial T_2^l}{\partial z}\right)_{z=2H,t} = h_a[T_2^l(z = 2H, t) - T_\infty] \tag{8}$$

$$\left(-k \frac{\partial T}{\partial z}\right)_{r>R,z=0,t} = h_a[T(r > R, z = 0, t) - T_\infty] \tag{9}$$

Boundary conditions 6 and 7 simply state that the temperature inside the substrate far away from the surface, as well as the temperature of the substrate surface far away from the splat region, remain unaffected by the melting and solidification process of the first splat and retain their initial value. Boundary conditions 8 and 9 account for convective losses through the top of the second splat and the top of the substrate surrounding the splat, respectively.

It has been found in studies of single-droplet splats [10, 11, 15, 16] that it is important to account for the presence of contact resistance in the heat-transfer modelling of the splat-cooling process. However, this contact resistance is very difficult to evaluate because of its variation with time and position. As an alternative, most investigators choose to quantify the contact resistance by the use of a constant heat-transfer coefficient (the reciprocal of the contact resistance). Therefore, the boundary condition for the interface between the two splats in terms of h_c, the contact heat-transfer

coefficient, is expressed as

$$\left(-k_1^{\mathrm{m}}\frac{\partial T_1^{\mathrm{m}}}{\partial z}\right)_{z=H,t} = h_{\mathrm{c}}[T_1^{\mathrm{m}}(z=H,t) - T_2^{1}(z=H,t)] \tag{10}$$

A matching condition analogous to Equation 10 is utilized at the interface to couple the substrate with the first splat

$$\left(-k\frac{\partial T}{\partial z}\right)_{r<R,z=0,t} = h_{\mathrm{c}}[T(r<R,z=0,t) - T_1^{\mathrm{m}}(z=0,t)] \tag{11}$$

The next issue to be discussed is that of the melting/freezing interface separating the solid from the liquid region. At this interface the following energy balance is satisfied

$$\rho_j^{\mathrm{s}} LV = \left(k_j^{\mathrm{s}}\frac{\partial T_j^{\mathrm{s}}}{\partial z}\right)_{z=z_{\mathrm{i}}} + \left(-k_j^{1}\frac{\partial T_j^{1}}{\partial z}\right)_{z=z_{\mathrm{i}}} \tag{12}$$

The subscript i denotes the melting/freezing interface, V is the velocity of this interface, and L is the latent heat of fusion. A melting interface moving downward has a negative value of V, while a freezing interface moving upward has a positive value of V.

Different approaches are taken to treat the melting and freezing interfaces. In the classical equilibrium treatment of a phase change interface, this interface is defined by the melting/freezing temperature of the material, T_{f}, and its propagation velocity is limited by Equation 12 (the rate at which the heat generation at the interface is conducted away in the liquid and solid regions).

For the melting interface, it is assumed that the melting will take place according to the above equilibrium condition. Therefore, the additional boundary condition at the interface is

$$T_1(z=z_{\mathrm{i}},t) = T_{\mathrm{f}} \tag{13}$$

The interface velocity is directly determined by an energy balance at the interface expressed in Equation 12.

For the freezing interface, however, the classical equilibrium treatment does not account for the presence of undercooling in the melt which is of great importance to rapid solidification processes such as the splat-quenching problem under investigation. To model the undercooling, a freezing kinetics relationship between the amount of undercooling and the velocity of propagation of the freezing front is needed. A common relationship of this kind postulates a linear dependence between the freezing front propagation velocity and the amount of undercooling [10, 11, 15, 16, 19, 20]

$$V = K_{\mathrm{f}}(T_{\mathrm{f}} - T_{\mathrm{i}}) \tag{14}$$

where K_{f} is a freezing kinetics coefficient, T_{f} is the equilibrium freezing temperature of the material and T_{i} is the actual interface temperature. Obviously, the difference $T_{\mathrm{f}} - T_{\mathrm{i}}$ defines the amount of undercooling. If undercooling exists and T_{i} is below T_{f}, Equation 14 will result in a rate of latent heat release in excess of that which can be conducted away from the interface (Equation 12). In this limit, the propagation of the solidification front is said to be controlled by the freezing kinetics. The rapid propagation of the freezing interface will cause its heating and subsequent retardation of solidification. As the freezing interface temperature approaches the equilibrium freezing temperature, the solidification becomes heat-transfer limited.

The numerical solution of the aforementioned mathematical model was obtained with the finite difference method. To this end, the substrate was overlaid with a network of M points in the radial direction and N points in the axial direction. Both the grid sizes Δr and Δz were allowed to vary depending on the spatial position. The finite differencing of the heat-conduction model in the substrate was obtained using a control volume formulation [10, 11, 21] and solved by utilizing the ADI method [22]. No further details on the control volume formulation or the ADI method are included here for brevity, for they can be found in the aforementioned literature.

The control volume method was also used to discretize the unidirectional heat-conduction model in the splat. The splat was overlaid with a unidirectional uniform grid (in the axial direction) consisting of I grid points for one splat. The discretized equations of the splat were cast in tridiagonal form and solved with the Thomas algorithm [22].

To account for the sudden change in the value of the thermophysical properties across the melting/freezing interface, the following procedure [23] was adopted. The control volume containing the melting/freezing interface was subdivided into two regions, a solid region and a liquid region. Three (instead of one) grid points were placed in this control volume. One at the interface location, one at the centre of the solid region, and one at the centre of the liquid region. These three points satisfied the following equations (which were discretized utilizing the control volume method, as well)

$$\left(-k_j^{\mathrm{s}}\frac{\partial T_j^{\mathrm{s}}}{\partial z}\right)_{\mathrm{b}} + \left(k_j^{\mathrm{s}}\frac{\partial T_j^{\mathrm{s}}}{\partial z}\right)_{\mathrm{i}} = \rho_j^{\mathrm{s}} c_j^{\mathrm{s}}\frac{\partial T_j^{\mathrm{s}}}{\partial t} \tag{15}$$

$$\left(-k_j^{\mathrm{s}}\frac{\partial T_j^{\mathrm{s}}}{\partial z}\right)_{\mathrm{i}} + \left(k_j^{1}\frac{\partial T_j^{1}}{\partial z}\right)_{\mathrm{i}} = -\rho_j^{\mathrm{s}} LV \tag{16}$$

$$\left(-k_j^{1}\frac{\partial T_j^{1}}{\partial z}\right)_{\mathrm{i}} + \left(k_j^{1}\frac{\partial T_j^{1}}{\partial z}\right)_{\mathrm{t}} = \rho_j^{1} c_j^{1}\frac{\partial T_j^{1}}{\partial t} \tag{17}$$

In the above equations subscripts i, b, and t stand for interface, the bottom of the control volume containing the interface and the top of the control volume containing the interface. Equations 15 and 17 are energy balances in the solid and liquid regions of the control volume containing the interface, respectively. Equation 16 is the interface energy balance.

Based on previous studies [15, 16], $M \times N = 70 \times 70$ grid points in the substrate and $I = 100$ points in each of the two droplets of the splat were chosen. Adding five points in either direction of the substrate left the results unaltered. A very fine time step ($\Delta t = 10^{-12}$ s) was used at the earlier stages of the

melting/freezing phenomenon. At later times the time step was gradually increased to reflect the fact that the heat-transfer process had slowed down. This task was performed by trial and error. The initial size of the time step was chosen to be small enough so that the maximum change in temperature within one time step is within 0.1%.

The numerical computation marched forward in time as follows. First, it was assumed that a very small region of the first splat (0.01% of the splat thickness) was already melted to avoid extremely large values of the interface velocity due to the very small time step at $t = 0$. The effect of the thickness of this assumed initially melted region on the results was investigated by comparing the findings of two different initially melted regions: one 0.01% and the other 0.02% of the splat thickness. There was no difference in the interface position and velocity after 0.01 μs, which is a very short time compared to the approximate duration of the remelting process (10 μs).

The melting interface was moved downwards a distance equal to the product of the interface velocity and one time step. The velocity of the melting interface was determined from Equation 12 using the temperatures obtained from the previous time step. Utilizing the updated physical conditions the solution was advanced by one time step using the ADI method and the Thomas algorithm. If the change of the temperature field between the current time step and the previous time step was very small, the size of the future time step was increased accordingly to speed up the calculation and the cycle was repeated. The melting of the first splat progresses downwards until the interface velocity reaches zero.

Freezing of the melted region of the first splat was initiated when the temperature of the interface reached a value below the prescribed degree of undercooling. The freezing process was treated in a manner identical to that of the melting process except that the interface velocity was determined by the freezing kinetics relationship, Equation 14. This procedure was followed until the melted region in the first splat solidified entirely (the interface reached the top of the first droplet). The computation was terminated some time after the solidification of the first droplet was completed. The numerical code typically required about 1 CPU hour to run one case on an IBM 3090/300J.

3. Experimental procedure

The main goal of the experimental study was to demonstrate the remelting of an initial metal deposit by the impaction of a second liquid-metal droplet. Consequently, the experimental apparatus was designed to generate two identical liquid-metal droplets and deposit them sequentially on a solid substrate.

The solid surface upon which the droplets impacted was a clean, smooth copper plate of sufficient thickness (6.0 mm) to act as an infinitely thick substrate for the duration of the splat-quenching process. The main component of the experimental apparatus was a droplet generator shown schematically in Fig. 2 which was

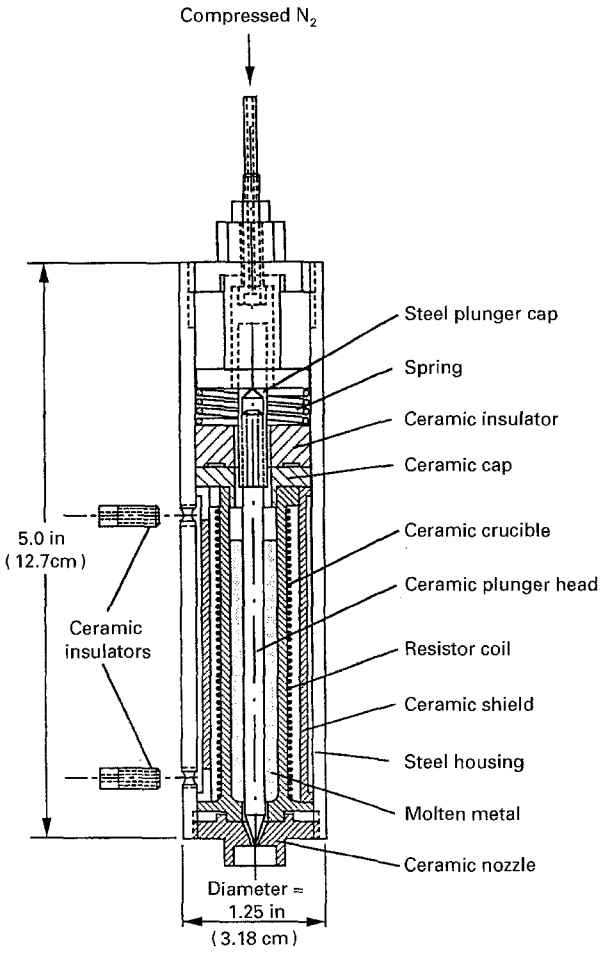

Figure 2 Schematic diagram of the molten metal droplet generator.

designed for this study to perform two functions: first, melt and superheat the metal under investigation and, second, generate a sequence of two liquid-metal droplets which were as nearly identical as possible. Within the droplet generator, metal was melted in a cylindrical ceramic crucible via resistive heating. Further details of the design and repeatability of the droplet generator have been previously published [16], and therefore will not be presented here.

To produce sequences of droplets with zero initial velocity, the droplet generator was pressurized slowly with nitrogen gas to produce a sphere of molten metal which would then break off under its own weight and fall freely to impact the substrate below. Once the initial droplet fell, the second droplet required approximately 5 s to form and break off. All droplets in this study were approximately 3.0 mm diameter and were released from a height of 219 mm which resulted in an impact velocity of 2.1 $m\,s^{-1}$. The initial droplet temperature was measured with a type K thermocouple inserted in the liquid metal exposed at the generator nozzle. It was determined that the droplets cooled about 3 °C during free fall based on a simple lumped capacitance thermal model using an empirical correlation for the convective loss from a sphere [24].

The material used in the experimental study was eutectic tin–lead solder. A eutectic composition was chosen for study because the theoretical model assumes a distinct liquid/solid interface (no mushy zone)

which is consistent with pure materials or eutectic alloys. Tin–lead solder was chosen due to its low melting point (183° C) and its oxidation resistance under normal atmospheric conditions when compared to pure metals. Also, the sharp contrast of the lead-rich and tin-rich phases aid in the identification of microstructural boundaries under metallographic examination using optical microscopy.

The only parameter which was varied in the experimental study was the amount of initial superheat, ΔT_{sup}. Three different values were used: $\Delta T_{sup} =$ 12, 57 and 87 °C. Four or five double splat pairs were deposited for each value of ΔT_{sup}. The solidified splats were easily removed from the substrate and weighed with a precision balance. The mass of the splat, together with the density of the liquid metal, were used to determine approximately the diameter of the droplets by assuming that the first and second droplets were identical spheres. To determine the diameter of the solidified splat, D, a digital caliper was used to take measurements at 0°, 45°, 90° and 135° about the deposit centre. These data, which had a measurement error of $\pm$ 0.03 mm and a maximum standard deviation of 1.8%, were averaged to determine D.

Once removed from the substrate, the solidified splats were mounted in an epoxy material which cures at room temperature to form a hardened transparent cylinder surrounding the specimen. This mounting material prevents the malleable splats from distortion due to handling, provides a convenient means to hold the specimen during metallographic grinding and polishing, and encases the splat surface preventing oxidation. Once the mounting material hardened, the specimens were wet ground with silicon carbide papers in the order 60, 120, 240, 320, 400, 800 and 1200 grit. The papers were attached to a rotating wheel and were lubricated with a continuous stream of water to wash away particles removed from the specimen surface and to provide cooling so that frictional heating did not affect the microstructure. Each specimen was ground in a plane parallel to the z-axis producing a cross-section through its centre analogous to that shown for the theoretical model in Fig. 1. After grinding, the specimens were polished with 5.0, 0.3 and 0.05 μm aluminium oxide powder in distilled water on a long-nap polishing cloth mounted to a rotating wheel. Between each grinding and polishing step the samples were cleaned ultrasonically with distilled water. The samples were then etched with a solution of (by volume) eight parts glycerin, one part acetic acid and one part nitric acid to enhance the phase boundaries and regions where a clear interface remained between the first and second deposit due to the absence of remelting. Specimens were examined with a Nikon Epihot optical microscope capable of 1000 × magnification. A representative specimen with the most clearly identifiable microstructure was chosen for each value of ΔT_{sup} for detailed study. Black and white photomicrographs of each were produced with a Polaroid Model 545 4 × 5 film holder mounted to the microscope.

4. Results and discussion

In the discussion of results, the numerical findings, including the impact of parameter variation, will be presented first. The experimental results focusing on the macro- and microstructure of the double-splat structure are presented subsequently. In all cases emphasis will be placed on the occurrence and effect of remelting.

As mentioned earlier, each droplet in the splat was approximated with a disc, such that the overall splat consisted of two identical discs as shown in Fig. 1. The dimensions of each disc were determined based on the experimental observations. To this end, the spread factor (the ratio of the disc diameter, D, to the spherical droplet diameter, d, prior to impact) $\xi = D/d = 4.1$, was utilized. Equating the mass of the spherical droplet to the mass of the disc for the above value of ξ yielded the height to diameter ratio of a single disc for the numerical simulation $H/D = 0.0097$. The behaviour of the lead, tin and aluminium, and eutectic solder splats on a copper substrate was examined in the numerical simulations.

The initial temperature of the substrate was room temperature ($T_\infty = 25$ °C). The initial temperature of the bottom splat depends on the time interval from the completion of the solidification of the bottom splat to the moment at which the top splat contacts with the bottom splat. For the lead, tin, and aluminium splats, the initial temperature of the bottom splat, which was expressed in terms of ΔT_1 in Equation 3, is taken to be $\Delta T_1 = 2$ °C because it is assumed that the top droplet contacts the bottom splat a short time after the solidification process of the bottom splat is completed. For the solder splat simulating the experimental conditions, on the other hand, the second droplet always impacted on to the bottom splat a few minutes after the first droplet impacted on to the substrate. To reflect this experimental situation, the initial temperature of the bottom splat is assumed to be a bit higher than the room temperature ($T_1 = 30$ °C), which results in $\Delta T_1 = 153$ °C for the solder splat.

The initial temperature of the second droplet is determined by the assigned value of superheat ($\Delta T_{sup} = T_0 - T_f$). Three different values of superheat, i.e. 100, 300, and 500 °C, were examined for the lead, tin, and aluminium splats to investigate the effect of the amount of superheat on the remelting process of the first splat. For the solder splat, the values of superheat measured from the experiments, i.e. $\Delta T_{sup} = 12$, 57 and 87 °C were directly utilized to simulate the experiment. An additional case with the high superheat $\Delta T_{sup} = 300$ °C was examined. It is worth noting that the computation for the solidification of the remelted region was continued only for the lead, tin, and aluminium splats with the value of $\Delta T_{sup} = 300$ °C.

As mentioned previously, severe undercooling is present in the process of splat cooling. Based on earlier experimental measurements [10, 11, 15, 16], the value of undercooling $(T_f - T_i)_{t'=0} = 40$ °C was assigned for all numerical experiments. According to the literature [10, 11, 15, 16], the value for the contact heat-transfer coefficient between the splat and the substrate

TABLE I Values of all the parameters used in the numerical study

		k(W m^{-1} K^{-1})	ρ(kg m^{-3})	c(J kg^{-1} K^{-1})	L(J kg^{-1})	T_f(°C)
copper		397.0	8960	386.0		
Lead:	solid	34.9	11680	129.8	23220	327.50
	liquid	15.4	10678	152.0		
Tin	solid	73.2	7300	226.0	59033	231.97
	liquid	30.0	7000	250.0		
Aluminium:	solid	238.0	2700	917.0	397750	660.37
	liquid	94.0	2385	1080.0		
Eutectic lead–tin	solid	48.0	8420	176.0	46000	183.00
solder:	liquid	25.0	8218	238.0		

d	3.0 mm
D	12.3 mm
H	119.0 μm
h_a, for top surface of splat	20.0 W m^{-2} K^{-1}
h_a, for top surface of substrate	8.0 W m^{-2} K^{-1}
h_c, for between splat and substrate	1.0×10^4 W m^{-2} K^{-1}
h_c, for between splats	1.0×10^6 W m^{-2} K^{-1}
K_f	0.05 m s^{-1} K^{-1}

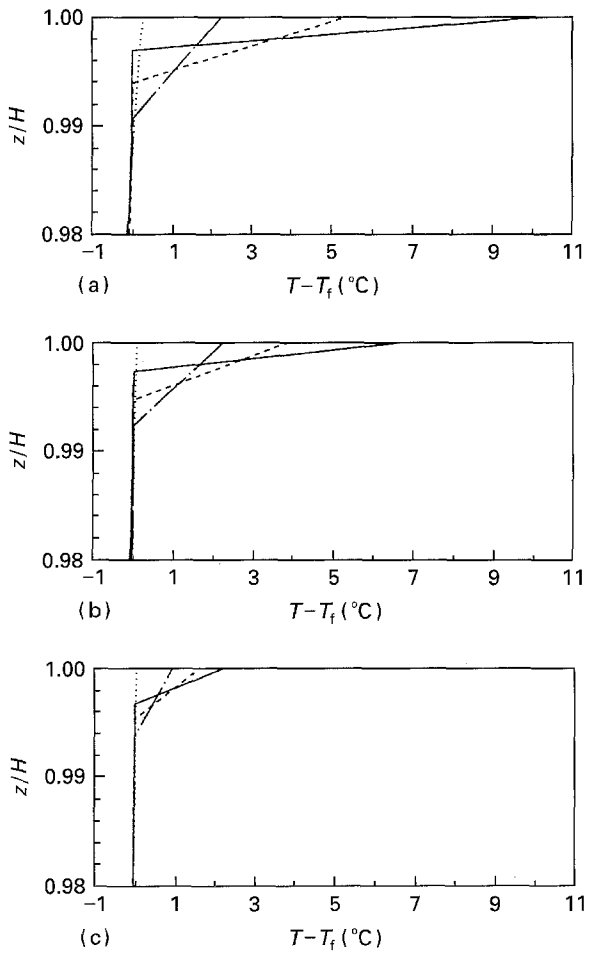

Figure 3 The temperature distribution of the bottom splat during the melting process for $\Delta T_{sup} = 300$ °C for (a) lead, (b) tin, (c) aluminium. (a) (—) 0.088 μs, (– – –) 0.58 μs, (—·—) 2.48 μs, (· · ·) 10.74 μs. (b) (—) 0.089 μs, (- - -) 0.53 μs, (–·–) 1.58 μs, (· · ·) 9.58 μs. (c) (—) 0.31 μs, (– – –) 0.78 μs, (—·—) 1.85 μs, (· · ·) 8.36 μs.

has been found to range from 10^4–10^6 W m^{-2} K^{-1}. A high value of the contact heat-transfer coefficient for the interface between the two splats, $h_c = 1.0 \times 10^6$ W m^{-2}K^{-1}, was selected because the occurrence of the remelting of the first splat, which has been verified by experimental observations, implies very low heat resistance at the contact surface. On the other hand, a low value of $h_c = 1.0 \times 10^4$ Wm^{-2} K^{-1} is used for the contact heat-transfer coefficient between the splat and the substrate. The values of all the parameters (thermophysical properties of metals and transport coefficients) utilized in the numerical study are listed in Table I. These are all realistic values, and they are held fixed throughout this study.

The temperature distribution across the splat thickness during the remelting of the bottom splat in the case of $\Delta T_{sup} = 300$ °C is shown in Fig. 3 for the bottom splat and in Fig. 4 for the top splat. For the sake of clarity, only the top portion of the bottom splat (where the melting interface exists) is shown in Fig. 3 for three different splat metals. The location of the melting front in Fig. 3 is marked by cusps in the curves corresponding to times where melting is present. As time progresses, the melting front propagates downwards until the velocity of the melting interface, expressed by Equation 12, becomes zero, which means that the heat transferred from the liquid region into the melting interface is equal to the heat transferred away from the melting interface to the solid region. The temperature gradient in the liquid region, which is directly related to the magnitude of the interface velocity, is very large at the early stage of the melting process. It then gradually decreases because the available amount of superheat from the top droplet decreases as time progresses. On the other hand, the temperature in the solid region remains almost constant at the melting temperature of the splat (Fig. 3).

The temperature distributions of the lead and tin splat are similar; however, the temperature of the aluminium splat decreases more rapidly by comparison (Figs 3 and 4). For example, the temperature $(T - T_f)$ of the top of the aluminium splat at $t = 0.31$ μs is only 2 °C, but the temperatures of the lead splat at $t = 0.58$ μs and the tin splat at $t = 0.53$ μs are 5 and 4 °C, respectively. The reason can be explained by the relatively large value of the latent heat of aluminium compared to that of lead and tin. As can

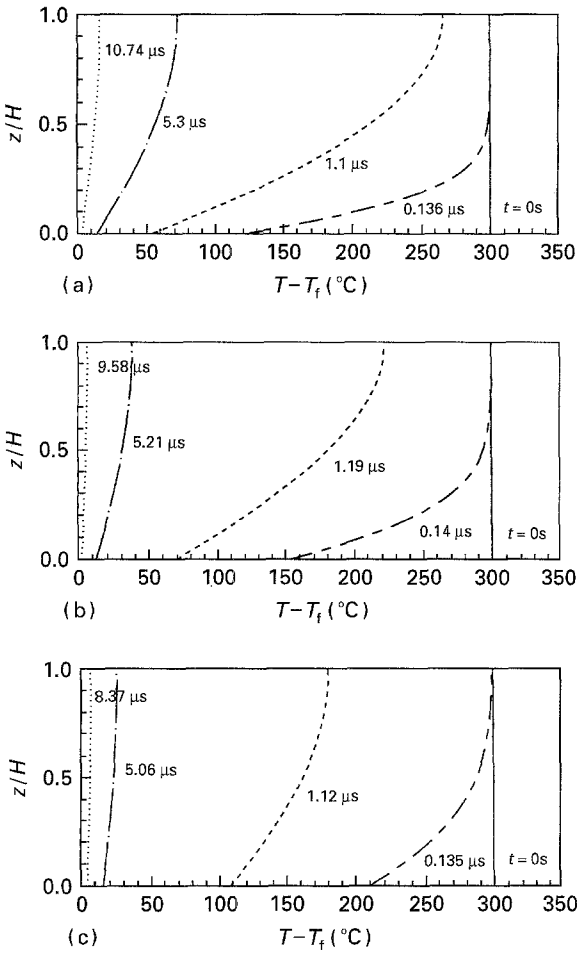

Figure 4 The temperature distribution of the top splat during the melting process for $\Delta T_{sup} = 300\,°C$ for (a) lead, (b) tin, (c) aluminium.

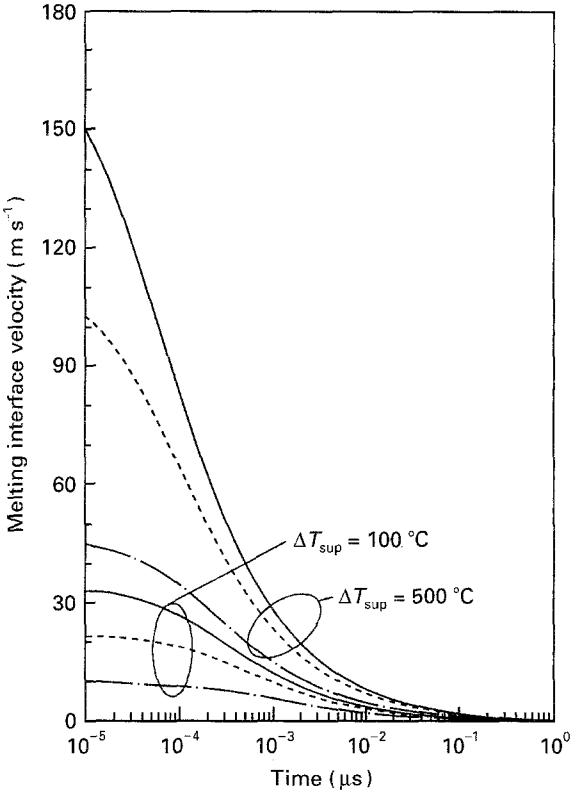

Figure 5 The melting interface velocity for $\Delta T_{sup} = 100$ and 500 °C for (—) lead, (– – –) tin, and (–·–) aluminium.

be found in Table I, the latent heat of aluminium is 7 and 17 times larger than that of tin and lead, respectively, which implies that more heat is required for the melting process of aluminium. More heat absorption at the melting interface results in the rapid decrease of the temperature in the liquid region because the amount of superheat provided by the top droplet is limited.

The temperature distribution across the entire top splat thickness in Fig. 4 shows the cooling process of the superheated liquid-metal droplet due to the heat-absorbing melting process occurring in the bottom splat. We observe that the cooling of the top droplet propagates up to half of the splat thickness at $t = 0.136$ μs in Fig. 4a. At practically the same time, the cooling effect propagates through the entire splat in Fig. 4c. The effect of the thermal conductivity of the three different splats on the speed of the cooling process can be clearly observed in Fig. 4. The temperatures $(T - T_f)$ of the top of the lead, tin and aluminium splats at $t = 1.1$, 1.19, and 1.12 μs are 265, 220 and 180 °C, respectively. This indicates that the cooling effect propagates faster in the order of aluminium, tin, and lead. Note that the ratios of thermal conductivities of liquid aluminium and tin to the thermal conductivity of liquid lead are 6.1 and 1.9, which means that conduction is the greatest in liquid aluminium, followed by conduction in liquid tin.

The melting interface velocity in the case of $\Delta T_{sup} = 100$ and 500 °C for three different splats is shown in Fig. 5. At the early stage of the melting process, the melting interface velocity is very high due to the high heat flux from the superheated top droplet. As time progresses, the cooling of the top splat results in the decrease of the heat flux to the melting interface which causes a decrease of the melting interface velocity. The melting interface velocity approaches zero until the equilibrium of the heat flux at the melting interface is established. Another important finding in this figure is the variation in the melting interface velocity among the three splats at the same superheat condition. As one would expect from the Equation 12, the melting interface velocity is inversely proportional to the latent heat of melting. This implies that the melting front for a material with a high latent heat does not proceed faster than that for a material with a lower latent heat. This is why the highest melting interface velocity in Fig. 5 is exhibited by lead which also features the lowest latent heat.

The melting interface position is shown in Fig. 6a for the lead, tin, and aluminium splats in the case of $\Delta T_{sup} = 100$ and 500 °C and in Fig. 6b for the solder splat. The behaviour of the melting interface position in Fig. 6a is analogous to that of the melting interface velocity shown in Fig. 5. The melting front advances more for higher superheats. The effect of the material properties is accentuated as the superheat increases from 100 °C to 500 °C (Fig. 6a). For the solder splat (Fig. 6b), remelting of the bottom splat is also predicted, except in the case of the lowest superheat $\Delta T_{sup} = 12\,°C$. At this superheat condition, the temperature of the top surface of the bottom splat in-

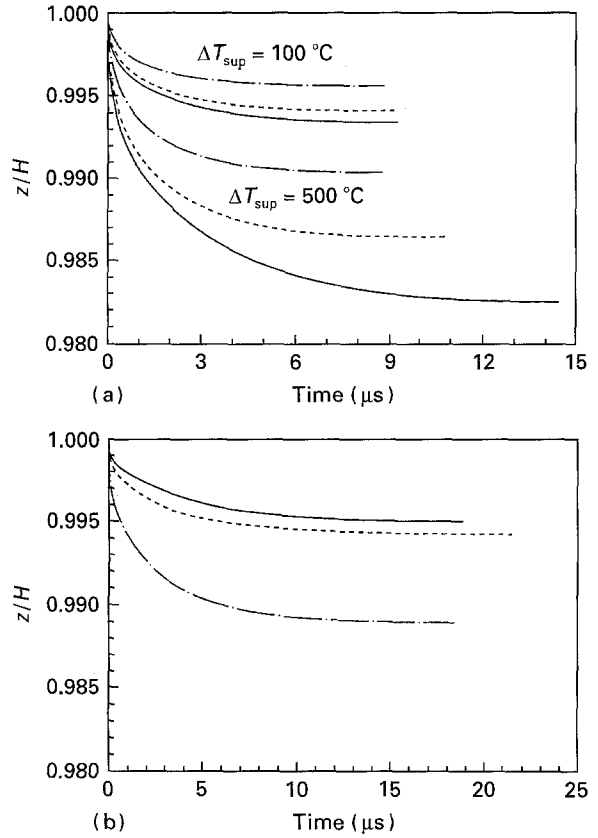

Figure 6 The propagation of the melting interface for (a) (—) lead, (– – –) tin, and (–·–) aluminium for ΔT_{sup} = 100 and 500 °C, (b) solder Q for ΔT_{sup} = (—) 57 °C, (– – –) 87 °C and (–·–) 300 °C.

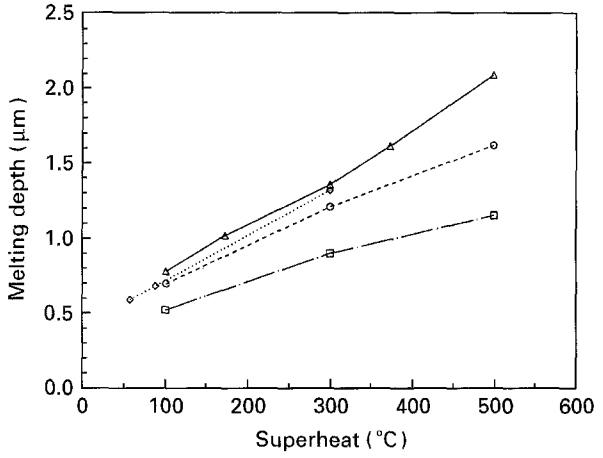

Figure 7 The relation between the melting depth and the superheat of the splat. (△) Lead, (○) tin, (□) aluminium, and (◇) solder.

creased up to 60 °C (below the melting temperature) and it subsequently decreased. This finding implies that the superheat of the second droplet needs to exceed a threshold value for the remelting to be initiated.

The relation between the amount of superheat of the second droplet and the melting depth for four different splats is shown in Fig. 7. The remelting depth increases almost linearly, regardless of the splat material, as the amount of superheat is increased. Considering the fact that the amount of superheat existing in many splat-cooling processes exceeds 100 °C, it is reasonable to anticipate the occurrence of remelting. This fact was also verified by the experimental observations

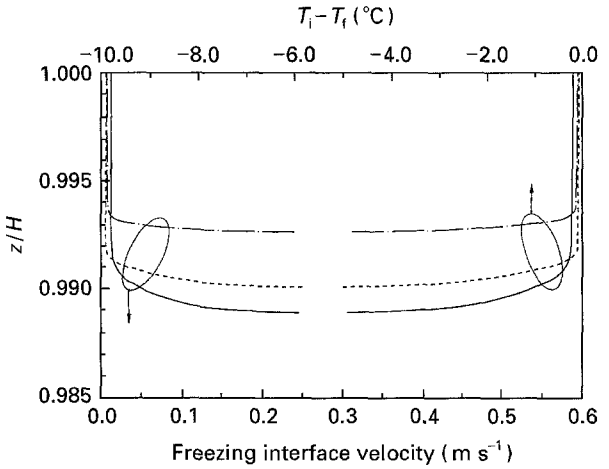

Figure 8 The freezing interface temperature and velocity, for (—) lead, (– – –) tin, and (–·–) aluminium.

of this study. As explained in connection with Figs 5 and 6, the melting front propagated the most in the case of lead, followed by the tin and aluminium. As shown in Fig. 7, the melting depth of the solder splat is between the melting depths of the lead and tin splats, because the solder is a lead and tin alloy.

The freezing interface temperature and velocity are shown in Fig. 8. All three splats exhibit a behaviour that is controlled by the freezing kinetics as expressed by Equation 14 at the initial stage of the solidification. The heat released at the freezing interface is not fully used to increase the freezing interface temperature because it is rapidly conducted away. A considerable amount of undercooling, which controls the freezing interface velocity, exists at this stage. As the undercooling decreases, the heat-transfer limited behaviour becomes apparent. This indicates an equilibrium between the heat released at the freezing interface and the heat conducted away from the freezing interface. The freezing interface temperature remains constant due to the establishment of the aforementioned balance between heat generation and removal at the freezing interface. The behaviour of the freezing velocity can be explained in a manner analogous to that of the freezing temperature because the shape of the freezing velocity curve is practically a mirror image of that of the freezing interface temperature curve. There is no significant variation in the behaviour of the freezing interface temperature or velocity for the three different splat materials except a small increase in undercooling and interface velocity for the lead splat due to the lower heat release at the freezing interface for this material.

The temperature history of the top of the bottom splat for three different materials is shown in Fig. 9. The behaviour is similar to that of the remelting/freezing interface because this interface is very close to the top surface of the bottom splat. The onset of solidification at the freezing interface is marked by the cusps in the temperature versus time curves. Prior to the initiation of solidification, the undercooling of the freezing interface is indicated by the rapid decrease of the temperature with time. At the onset of solidification, the temperature increases

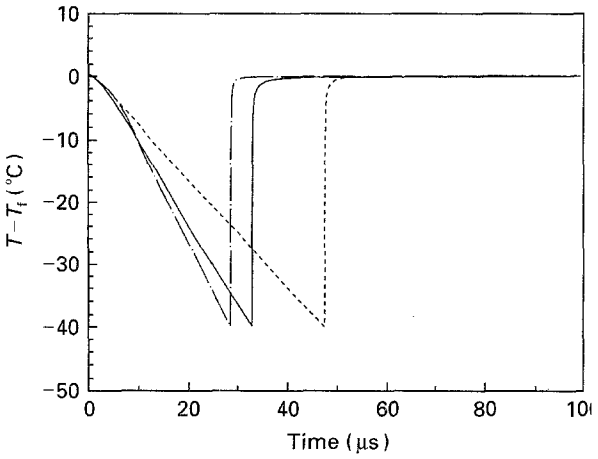

Figure 9 The temperature history of the top surface of bottom splat during the freezing process, for (—) lead, (– – –) tin, and (–·–) solder.

abruptly to the freezing temperature due to the heat release at the freezing interface, and remains almost constant thereafter.

The temperature field in the substrate for the three splat materials at approximately the same time is shown in Fig. 10. The isotherm, $T = 27.9\,^{\circ}C$, propagated to almost the same depth in the substrate for the lead and aluminium splats. On the other hand, a very small region of the substrate is affected by the tin splat. An explanation for this behaviour is the low freezing temperature of tin compared to that of aluminium and lead (note that the three cases in Fig. 10 correspond to the same amount of superheat). Also, the freezing process of the tin splat is still in progress at the time corresponding to Fig. 10, whereas it is completed for the lead and aluminium splats.

As mentioned earlier, the experimental phase of this study produced a representative tin–lead specimen for each value of superheat tested; namely, $\Delta T_{sup} = 12$, 57 and 87 °C. There are several reasons for close inspection of the splats after solidification, the most obvious being to investigate the effects of rapid solidification and remelting on microstructure. One may also observe the overall shape of the splat to ascertain what phenomena had occurred. Lastly, the splats can be inspected to determine if a clear interface exists between the first and second deposits, which would indicate that remelting did not occur.

Figs 11–13 are a collection of micrographs corresponding to the three superheat conditions. Figs 11j–13j in each case show an overall view of the splat with the originating region for Figs 11a–i to 13a–i. It is immediately evident that vast microscopic and macroscopic differences exist not only when comparing different splats, but also when comparing different regions of the same splat.

From a macroscopic point of view, one can observe that the assumption of thin discs for the theoretical model was appropriate for the central region of the splat; however, there is an accumulation of material around the outer edge. It is also clear that the amount of superheat drastically influences the extent of remelting and, hence, distortion of the initial deposit. In Fig. 11j the splat is of nearly uniform thickness except

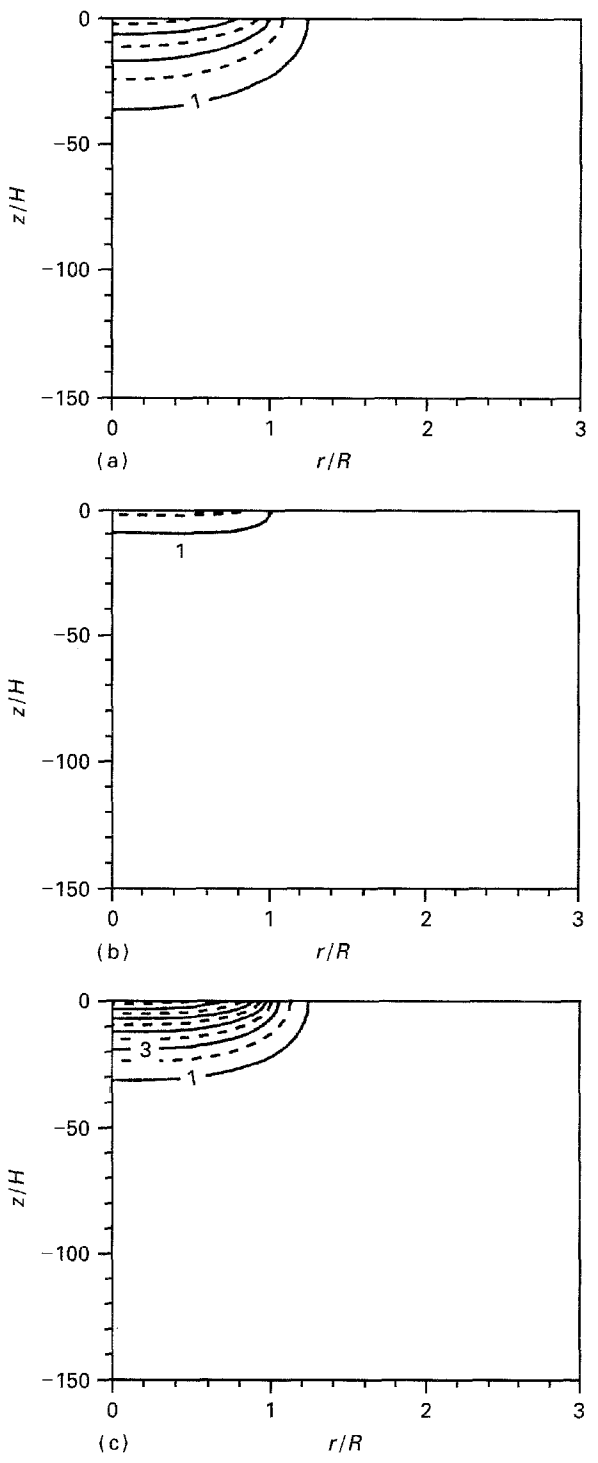

Figure 10 Transient isotherms in the substrate for $\Delta T_{sup} = 300\,^{\circ}C$ for (a) lead, (b) tin, (c) aluminium. (a) $t = 0.15$ ms, $1 = 27.9\,^{\circ}C$, $6 = 42.9\,^{\circ}C$, $\Delta T = 3.0\,^{\circ}C$. (b) $t = 0.13$ ms, $1 = 27.9\,^{\circ}C$, $2 = 30.9\,^{\circ}C$, $\Delta T = 3.0\,^{\circ}C$. (c) $t = 0.14$ ms, $1 = 27.9\,^{\circ}C$, $10 = 54.9\,^{\circ}C$, $\Delta T = 3.0\,^{\circ}C$.

for the thickening at the outer edge. The curvature of the bottom surface may be explained by the fact that the substrate was not fluxed prior to contact, resulting in poor adhesion between the deposit and the substrate. Thermal contraction upon cooling of the second droplet (after solidification) would cause the top surface of the initial deposit to be in tension and, therefore, curl upwards. There is a more pronounced thinning of the splat centre with increased superheat in Fig. 12j and a slight depression of the lower surface in the centre region. Fig. 13j exhibits the most drastic macroscopic variations which are certainly due to

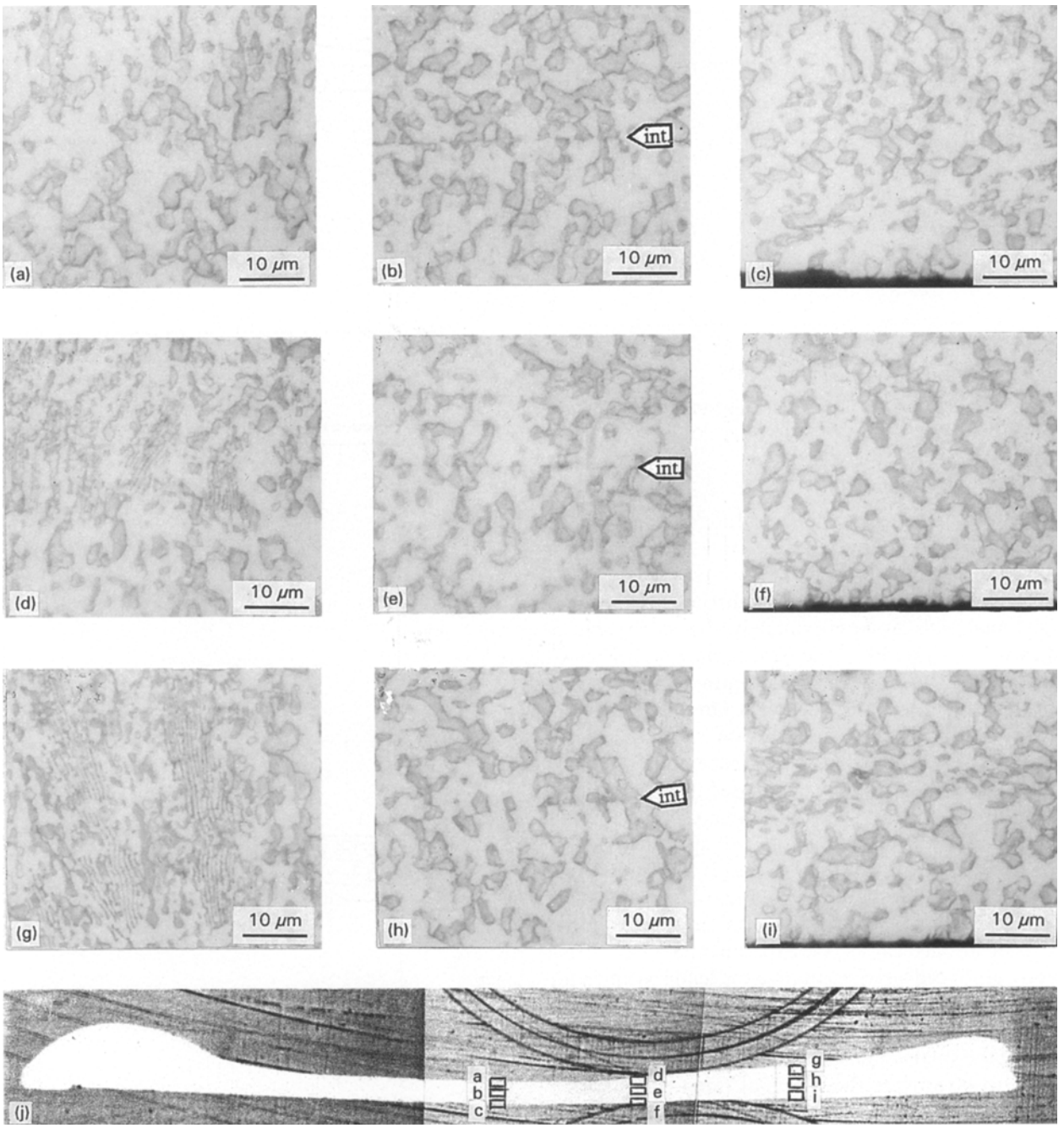

Figure 11 Solder splat microstructure in various regions (a–i), and the overall cross-section of the splat (j) with the origin of the regions in (a–i) for $\Delta T_{sup} = 12\,^{\circ}C$.

remelting. It appears that a portion of the centre region of the initial deposit may have remelted and flowed radially outward. It is also important to note that the dark line that appears in the lower portion of the splat in this figure does not correspond to an interface between the two deposits. Under closer examination at a radial position where such an interface does exist due to a lack of remelting, this dark line actually appears below the interface. By focusing the microscope above and below this line, it was clear that the heights of the prepared specimen were different in these two regions. This was most likely caused by preferential grinding and polishing due to hardness variations.

Some general comments concerning the microstructure of the tin–lead eutectic are necessary to understand the microscopic variations within the splats. It is common to categorize eutectic structures into three groups [25] : particle structures, colony structures and grain structures. This discussion will focus on particles and colonies. Phase particle structures are typically on the order of 10^{-1}–10^{1} μm in size. Their size and shape significantly impact the mechanical and physical properties of the eutectic aggregate. When optical microscopy is used, lead-rich particles appear as dark structures, while tin-rich particles appear light (Figs 11–13). It has been established [25] that the interparticle spacing, l, and the solidification rate, S, for an alloy can be related by an equation of the form $l^2S = \text{constant}$. Clearly, as the solidification rate increases, the interparticle spacing decreases, providing at least a qualitative tool to evaluate splat microstructure. Particles within the tin–lead eutectic can also be categorized by their shape. A lamellar

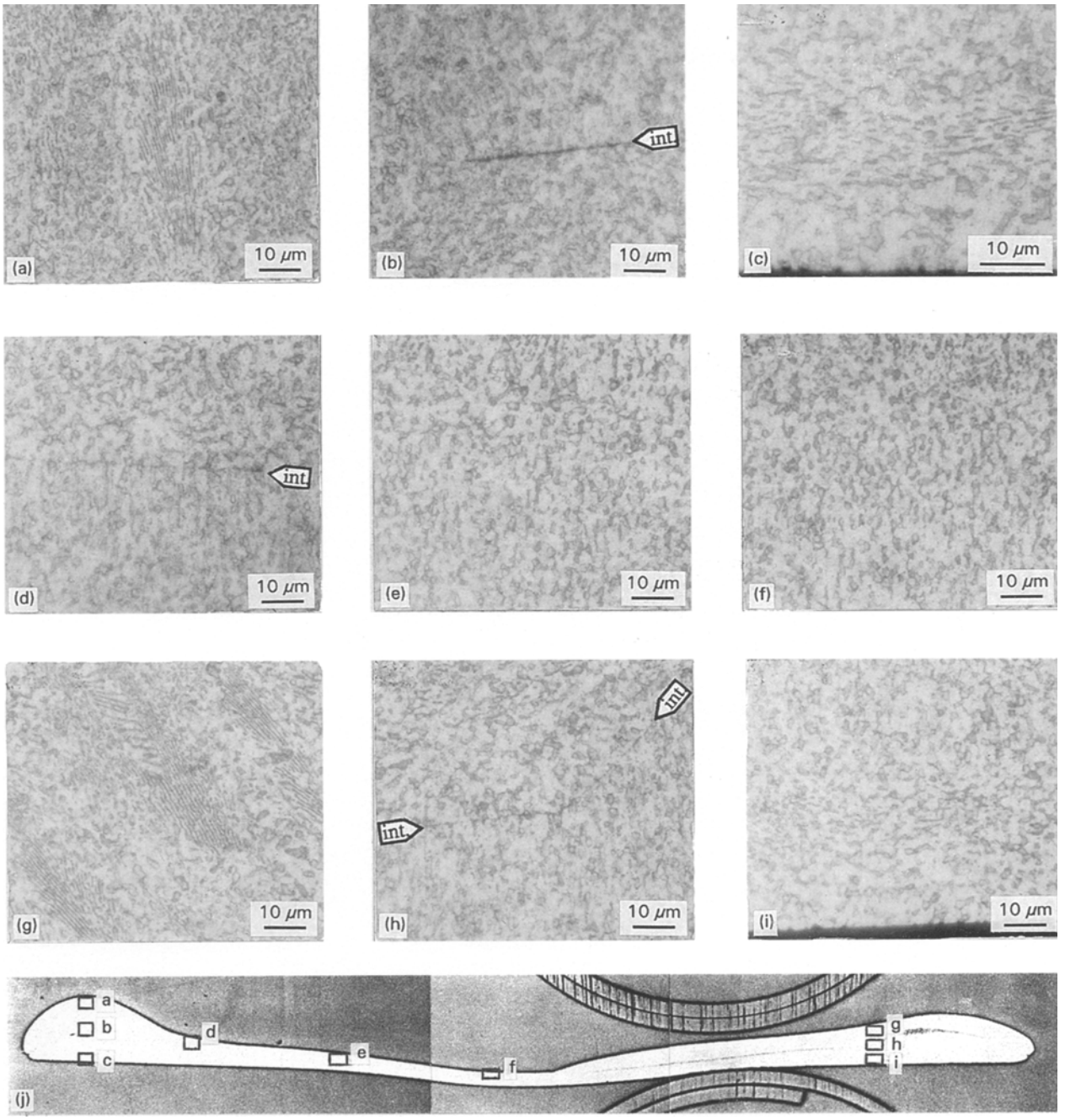

Figure 12 Solder splat microstructure in various regions (a–i), and the overall cross-section of the splat (j) with the origin of the regions in (a–i) for $\Delta T_{sup} = 57\,^{\circ}C$.

structure is a collection of parallel planes of alternating phases which appear as parallel, nearly linear segments in cross-section; for example, see Fig. 11g. In contrast, a globular structure is equiaxed or nearly the same size in all directions.

A eutectic colony is a collection of phase particles with a characteristic arrangement and is typically of the order of 10^1–10^3 μm in size. When a section is cut parallel to the solidification direction, the phase particles are typically arranged in a fan-like structure; for example, see Fig. 13h. In general, the tin–lead eutectic consists of lamellae or globules of lead-rich solution (dark) in a tin-rich matrix (light). High cooling rates are typified by globular structures, while low cooling rates are indicated by lamellar structures. Heat treatment at a temperature near the eutectic temperature, for example, a molten droplet impacting a solidified deposit, will convert lamellar structures to globules [25].

Microstructural variations at three radial locations for $\Delta T_{sup} = 12\,^{\circ}C$ are shown in Fig. 11a–i. For this case the initial droplet diameter and the final splat diameter were $d = 3.13$ mm and $D = 10.2$ mm, respectively. Globular structures in the centre section, Fig. 11a–c, indicate a high cooling rate throughout this area. By moving to the next radial location, Fig. 11d–f, finely spaced lamellar colonies begin to appear near the top surface, while the middle and lower sections contain globular structures. At the greatest distance from the centre, fan-shaped lamellar colonies are visible near the top surface of the splat (Fig. 11g), but again globules appear in the lower regions (Fig. 11h and i). Most importantly, the centre image for each radial location, Fig. 11b, e and h,

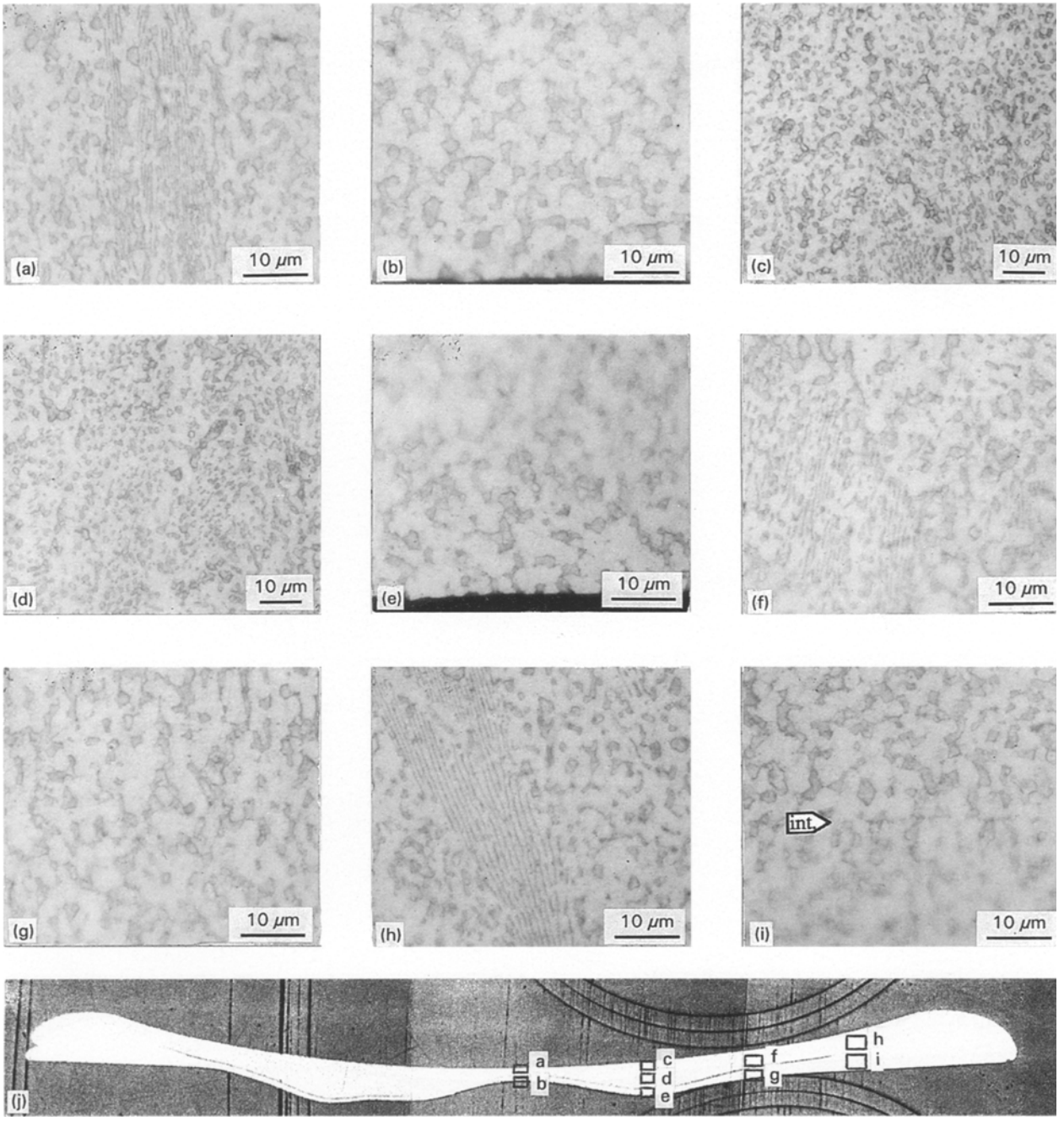

Figure 13 Solder splat microstructure in various regions (a–i), and the overall cross-section of the splat (j) with the origin of the regions in (a–i) for $\Delta T_{sup} = 87\,^{\circ}C$.

show a distinct interface separating the two deposits. Clearly, remelting did not occur with this low superheat value. The trend of globules to lamellar colonies along the top surface indicates a cooling rate which decreased with increasing distance from the splat centre. The orientation of the fan-shaped lamellae indicates that solidification proceeded in the positive z-direction, in support of the theoretical model.

Fig. 12a–i show the splat microstructure at multiple locations for $\Delta T_{sup} = 57\,^{\circ}C$. In this case the initial droplet diameter and the final splat diameter were $d = 3.25$ mm and $D = 10.7$ mm, respectively. The accumulation of material at the outer edge is examined at three heights above the substrate in Fig. 12a–c. A low cooling rate is indicated by the lamellar colony oriented in the z-direction at the top surface in Fig. 12a. A clear interface between the two deposits can be seen in Fig. 12b, while globular structures are apparent in Fig. 12c. The globules seem to become finer nearer the substrate, indicating an increasing cooling rate. By observing Fig. 12d–f, one concludes that an interface between the deposits does not exist for $r < R/2$, where R is the overall splat radius. Therefore, this superheat condition does result in significant remelting. The symmetry of the splat microstructure is demonstrated by the similarities between Fig. 12g–i and a–c. Also note the shape of the interface in Fig. 12h, which illustrates that the accumulation at the outer edge of the initial deposit is not remelted as molten material from the second droplet flows around this region.

The significant microscopic and macroscopic variations that exist for the condition $\Delta T_{sup} = 87\,^{\circ}C$ are shown in Fig. 13a–j. This condition resulted in initial droplet and final splat diameters of $d = 3.18$ mm and

$D = 10.7$ mm, respectively. Micrographs from the centre region, Fig. 13a and b, show the surprising occurrence of a vertically oriented lamellar colony at the top surface. For the other superheat conditions, the centre regions contained globular structures indicative of rapid cooling. Because the microstructure suggests slow cooling in this case, it is possible that the centre section remelted in its entirety and flowed such that the material separated from the substrate and the top surface solidified while this region of the splat was not in contact with the heat sink. The uniform fine globular structures and the lack of a distinct interface in Fig. 13c–e indicate that this portion of the splat experienced remelting and was in contact with the substrate when rapid solidification occurred. At a radial location of $r \approx R/2$, a reduced cooling rate is evident by the lamellar colonies in Fig. 13g, while remelting is still apparent in Fig. 13f. The clear interface in Fig. 13i shows that remelting does not exist for radial locations greater than $2R/3$ for this superheat condition. Lastly, a clear example of a fanshaped lamellar colony appears in Fig. 13h. The orientation of this colony and all other lamellar structures in this study substantiate the assumption that solidification propagates predominantly in the z-direction.

5. Conclusion

A combined theoretical and experimental study was reported on the splat cooling of two liquid-metal droplets impacting sequentially on a substrate focusing on remelting phenomena. Under conditions consistent with manufacturing applications where the initial superheat of the liquid metal is elevated, it has been proposed theoretically and demonstrated experimentally that an initial deposit is remelted by the subsequent impaction of molten material. The amount of initial superheat is clearly an important process parameter. It has also been shown that the variation of thermophysical properties, particularly the latent heat and the melting temperature, influences the degree of remelting. For the most part, the splat exhibited globular microstructure. Lamellar structures were observed near the top and the periphery of the splat indicating slower cooling rates at these locations.

Experimental findings supported, partially, the theoretical model assumptions that the splats could be represented by thin discs and that the heat transfer and solidification within the splat propagates in the axial direction only. However, the experiments showed that these assumptions are better suited for the centre region of the splat. Within this context, the one-dimensional model for the splat proved to be a useful predictive tool. Two important effects require discussion. First, the experimental data showed that the remelting varied radially depending on the amount of superheat. In the numerical model, the entire surface of the initial deposit had to be heated sufficiently to cause remelting. In an actual application, remelting may occur at a lower superheat condition because a reduced area, rather than the entire deposit surface, can remelt. Also, the simplified model assumes the liquid material experiences conduction heat transfer only. The drastic deformation of the impacting droplets in a short time interval suggests that significant convective heat transfer would be present, increasing the overall heat transport to the initial deposit from the second droplet. Accounting for the convective effects would require the inclusion of the complicated splashing behaviour of the droplet with computational fluid dynamics and heat-transfer modelling of the fluid region. Despite these issues, the proposed simple model can be employed to simulate the trend of the remelting phenomenon of multiple droplet splats and provide insight into process parameter optimization.

Acknowledgement

We thank Professor C.M. Megaridis, Mechanical Engineering Department, UIC, for bringing to our attention the phenomenon of remelting in the solidification of multiple droplet splats.

References

1. H. JONES, "Rapid solidification of metals and alloys", Monograph 8 (Institution of Metallurgists, London, 1982).
2. E. GUTIERREZ-MIRAVETE, PhD thesis, Massachusetts Institute of Technology (1985).
3. S. ANNAVARAPU, D. APELIAN and A. LAWLEY, *Metall. Trans.* **21A** (1990) 3237.
4. R. H. BRICKNELL, *ibid.* **7A** (1986) 583.
5. R. G. BROOKS, C. MOORE, A. G. LEATHAM and J. S. COOMBS, *Powder Metall.* **2** (1977) 100.
6. T. R. ANANTHARAMAN and C. SURYANARAYANA, *J. Mater. Sci.* **6** (1971) 1111.
7. P. PREDECKI, A. W. MULLENDORE and N. G. GRANT, *Trans. Metall. Soc. AIME* **233** (1965) 1581.
8. W. E. BROWER, Jr, R. STRACHAN and M. C. FLEMINGS, *AFS Cast Metals Res. J.* **6** (1970) 176.
9. M. G. SCOTT, *J. Mater. Sci.* **9** (1974) 1372.
10. G.-X. WANG and E. F. MATTHYS, *Int. J. Rapid Solid.* **6** (1991) 141.
11. *Idem, Int. J. Heat Mass Transfer* **35** (1992) 141.
12. P. H. SHINGU and R. OZAKI, *Metall. Trans.* **6A** (1975) 33.
13. D. E. ROSNAR and M. EPSTEIN, *Chem. Eng. Sci.* **30** (1975) 511.
14. P. V. EVANS and A. L. GREER, *Mater. Sci. Eng.* **98** (1988) 357.
15. T. BENNETT and D. POULIKAKOS, *J. Mater. Sci.* **29** (1994) 2025.
16. B. KANG, Z. ZHAO and D. POULIKAKOS, *J. Heat Transfer* **116** (1994) 436.
17. J. MADEJSKI, *Int. J. Heat Mass Transfer* **19** (1976) 1009.
18. *Idem, ibid.* **26** (1983) 1095.
19. C. G. LEVI and R. MEHRABIAN, *Metall. Trans.* **13A** (1982) 221.
20. T. W. CLYNE, *ibid.* **15B** (1984) 369.
21. S. V. PATANKAR, "Numerical heat transfer and fluid flow" (Hemisphere, New York 1981).
22. D. A. ANDERSON, J. C. TANNEHILL and R. H. PLETCHER, "Computational fluid mechanics and heat transfer" (Hemisphere, New York, 1984).
23. L. E. GOODRICH, *Int. J. Heat Mass Transfer* **21** (1978) 615.
24. W. RANZ and W. MARSHALL, *Chem. Eng. Progr.* **48** (1952) 141.
25. *ASM Metals Handbook*, Vol. 9 "Metallography and microstructures", 9th Edn (American Society for Metals, Metals Park, OH, 1979).

Received 13 July 1994
and accepted 5 April 1995